A parameterization of convective dust storms for models with mass-flux convection schemes

Florian Pantillon* and Peter Knippertz

Institut für Meteorologie und Klimaforschung, Karlsruher Institut für Technologie, Karlsruhe, Germany

John Marsham

Institute for Climate and Atmospheric Science, School of Earth and Environment, University of Leeds, Leeds, UK

Cathryn Birch

MetOffice@Leeds, School of Earth and Environment, University of Leeds, Leeds, UK

**Corresponding author address:* Florian Pantillon, Institut für Meteorologie und Klimaforschung, Forschungsbereich Troposphäre, Karlsruher Institut für Technologie, Kaiserstr. 12, 76128 Karlsruhe, Germany.

E-mail: florian.pantillon@kit.edu

ABSTRACT

Cold pool outflows, generated by downdrafts from moist convection, can generate strong winds and therefore uplift of mineral dust. These so-called "haboob" convective dust storms occur over all major dust source areas worldwide and contribute substantially to emissions in northern Africa, the world's largest source. Most large-scale models lack convective dust storms, because they do not resolve moist convection, relying instead on convection schemes. We suggest a parameterization of convective dust storms to account for their contribution in such large-scale models. The parameterization is based on a simple conceptual model, in which the downdraft mass flux from the convection scheme spreads out radially in a cylindrical cold pool. The parameterization is tested with a set of Unified Model runs for June and July 2006 over West Africa. It is calibrated with a convection-permitting run, and applied to a convection-parameterized run. The parameterization successfully produces the extensive area of dust-generating winds from cold pool outflows over the southern Sahara. However, this area extends farther to the east and dust generating winds occur earlier in the day than in the convection-permitting run. These biases are due to biases in the convection scheme. It is found that the location and timing of dust-generating winds are weakly sensitive to the parameters of the conceptual model. The results demonstrate that a simple parameterization has the potential to correct a major and long-standing limitation in global dust models.

1. Introduction

In a thunderstorm, the melting, evaporation, and sublimation of hydrometeors generate downdrafts that form a spreading cold pool at low levels (Byers 1949). The cold pool is denser than its environment and therefore spreads as a density current (e.g., Simpson 1999). The cold pool plays a dual role in the life cycle of the thunderstorm: it increases the low-level atmospheric stability and locally inhibits convection, but additionally lifts the surrounding, warmer air and triggers new convective cells (Byers 1949).

The cold pool outflow creates a front of wind gusts at its leading edge. Over arid grounds, the wind gusts can be strong enough to lift mineral dust. This process was first documented in peer-reviewed literature for Karthoum and described as “haboob” (Sutton 1925). Since then, haboobs have been reported over all major sources of mineral dust worldwide (see Knippertz 2014, and references therein). Dust uplift is found in cold pool outflows of different space and time scales: mesoscale convective systems (Houze 2004) can produce long-lived haboobs (Roberts and Knippertz 2014); small, strong downdrafts (microbursts, Fujita 1985) can produce short-lived haboobs (Miller et al. 2008); even small cold pools from precipitating congestus can produce dust uplift (Marsham et al. 2009). As all processes are related to convection, they are referred to as convective dust storms.

Convective dust storms of different origins have been observed over the Sahara during recent field campaigns: created by orographic convection over the northwestern Sahara (during SAMUM, Knippertz et al. 2007); embedded within the monsoon flow over the southern Sahara (during AMMA, Flamant et al. 2007; Bou Karam et al. 2008) and over the western Sahara (during GERBILS, Marsham et al. 2008b); and over the central Sahara, from locally generated moist convection, as well as mesoscale convective systems that propagate from the Sahel (during FENNEC, Marsham et al. 2013b; Allen et al. 2013). Observational (Marsham et al. 2008b, 2013b) and modeling studies (Heinold et al. 2013) suggest that convective dust storms contribute a large fraction of dust emission over the Sahara in summer. The Sahara is the main source of mineral dust worldwide, and convective dust storms may contribute to the local and remote impacts of Saharan dust on health, oceanic biochemistry, and atmospheric dynamics (see Knippertz and Todd 2012, for a review of mineral dust over the Sahara).

Investigating the systematic impact of convective dust storms is challenging: the ground observation network is sparse over the Sahara, and convective clouds often hide dust in satellite observations (Heinold et al. 2013; Kocha et al. 2013). Furthermore, most operational models lack convective dust storms (Marsham et al. 2011; Garcia-Carreras et al. 2013), since they do not explicitly resolve convection and rely on parameterization schemes. Parameterization schemes lack microbursts, because they do not account for subgrid-scale winds. Parameterization schemes also lack mesoscale convective systems, because they do not account for grid-scale organization of convection (e.g., Knippertz and Todd 2012). A parameterization of convective dust storms is needed to account for their contribution to dust uplift in large-scale models.

Several authors have parameterized wind gusts according to convective downdrafts: Nakamura et al. (1996) assumed conservation of horizontal momentum in downdrafts to compute peak wind gusts in numerical weather prediction models; Redelsperger et al. (2000) defined subgrid gustiness as a function of the downdraft mass flux to enhance surface fluxes in global circulation models; Cakmur et al. (2004) scaled a probability distribution of subgrid wind with the downdraft mass flux to compute dust uplift in global circulation models. Building on these previous studies, we suggest a parameterization of subgrid winds for dust uplift based on the downdraft mass flux of a convective parameterization scheme. Our parameterization aims at remaining simple, in order to be applied online or offline to any model with mass-flux convection scheme. It contrasts with the integrated approach of Hourdin et al. (2014), which improves the representation of wind and dust emissions in a global model – although it does not address the issue of convective dust storms – but requires a complete modification of subgrid parameterization schemes. Our parameterization also complements statistical downscaling methods, which improve dust emissions in global models but still lack the contribution from convective dust storms, such as the one by Ridley et al. (2013).

Section 2 describes the configuration of the model runs used to formulate the parameterization, compares their representation of cold pools and dust generating winds, and details the reference used to calibrate the parameterization. Section 3 explains and illustrates the conceptual model of the parameterization and its tuning. Section 4 gives the results of the parameterization for both the geographical distribution and diurnal cycle. Finally, Section 5 concludes the paper and discusses perspectives for future work.

2. Model runs

a. Configuration

The parameterization of convective dust storms is based on a set of model runs with the UK Met Office Unified Model. The Unified Model uses a seamless approach, from weather forecast to climate projection and from limited area to global domain (Walters et al. 2011). In the framework of the Cascade project, the model was run in a limited area configuration over West Africa at different spatial resolutions, with and without parameterisations of moist convection, and for different time periods during the summer 2006. The Cascade project allowed an investigation of the representation of tropical convection (Pearson et al. 2010, 2014; Birch et al. 2014a), its impact on the monsoon (Marsham et al. 2013a; Birch et al. 2014b), and its impact on dust emission (Marsham et al. 2011; Heinold et al. 2013).

The present study is mainly based on two runs with 4-km and 12-km grid spacings for the 60-day period 1 June to 30 July 2006. Diagnostics for convective mass fluxes, which are essential for the formulation of the parameterization of convective dust storms, were saved out during this time period only. Additional runs for the 10-day period 25 July to 3 August 2006 are also discussed, because the model was run at higher resolution with 1.5-km grid spacing for this time period, in addition to the 4-km and 12-km grid spacings. As convective mass fluxes were not saved out for this 10-day period, the additional runs cannot be used for the parameterization of convective dust storms. The relevant characteristics of the different runs are summarized in Table 1.

The model was run over limited area domains on a rotated cylindrical grid. Figure 1 illustrates the orography, soil fraction, and surface roughness over the 12-km domain. Figure 1a further displays the 4-km and 1.5-km domains. Operational analyses from the European Centre for Medium-Range Weather Forecasts (ECMWF) provided the initial conditions and lateral boundaries for the 12-km runs (Table 1). The 12-km runs provided the lateral boundaries conditions for the nested 4-km runs. The 4-km run for the 10-day period in turn provided the lateral boundaries for the nested 1.5-km run. Terrain-following hybrid coordinates were used in the vertical, with 70 levels starting at 2.5 m in the 4-km and 1.5-km runs, and with 38 levels starting at 10 m in the 12-km run (Table 1). The model configuration is detailed in Pearson et al. (2010).

The 1.5-km and 4-km runs fundamentally differ in their representation of convection as compared to the 12-km run: the convection is permitted to develop explicitly with 1.5-km and 4-km grid spacings, while it is parameterized with 12-km grid spacing (Table 1). In the Unified Model, the parameterization of moist convection is based on a convective available potential energy (CAPE) closure (Gregory and Rowntree 1990). Following a parcel theory modified by entrainment and detrainment, an ensemble of subgrid convective clouds is described by updraft and downdraft mass fluxes. Updrafts are initiated if a layer is positively buoyant; ascent occurs until the parcel becomes negatively buoyant. In turn, downdrafts are initiated as a fraction of updrafts if a layer is negatively buoyant; descent occurs until the parcel becomes positively buoyant or too close to the surface.

b. Representation of cold pools

Figure 2 compares the representation of cold pools in the 1.5-km, 4-km, and 12-km runs on 31 July 2006 (10-day period, Table 1). The respective peak of the diurnal cycle of precipitation is illustrated; it occurs at 12 UTC in the 12-km run (Fig. 2g) instead of 17 UTC in the 1.5-km and 4-km runs (Figs. 2a,d). The parameterization scheme triggers convection too early in the 12-km run (Marsham et al. 2013a; Birch et al. 2014b; Pearson et al. 2014), which is a common and well-documented issue in tropical regions (Yang and Slingo 2001; Dai 2006; Nikulin et al. 2012; Bechtold et al. 2014). Note that the 3 runs are not expected to look the same at any particular time, because they are only constrained at the lateral boundaries. The panels in Fig. 2 are used for illustration purposes only.

In both the 1.5-km and 4-km run, convective cells produce strong precipitation above 10 mm h^{-1} (Figs. 2a,d). The evaporation, melting, and sublimation of hydrometeors create cold pools at low levels with temperature contrast above 5 K (Figs. 2b,e). The outflow of cold pools produces strong surface winds above 10 m s^{-1} (Figs. 2c,f). Convective cells produce small, circular cold pools, which grow and merge into larger, more complex structures. In contrast, the convection scheme produces weak precipitation below 10 mm h^{-1} in the 12-km run (Fig. 2g). The evaporation of precipitation is too weak and too widespread to produce distinct cold pools (Fig. 2h). The 12-km run therefore lacks high winds resulting from convective cold pool outflows (Fig. 2i).

This qualitative comparison suggests that the 4-km and 1.5-km runs offer a similar representation of convection and strongly contrast with the 12-km run. Earlier studies showed that convection in the 1.5-km and 4-km runs occurs with a good timing compared to satellite observations, while convection occurs too early in the 12-km run (Marsham et al. 2013a; Birch et al. 2014b; Pearson et al. 2014). Furthermore, the development and growth of convective organization is weakly sensitive to the resolution between the 1.5-km and 4-km runs (Pearson et al. 2014). Weisman et al. (1997) also found that the structure and evolution of mesoscale convective systems varied little between runs with 4-km and 1-km grid spacing, although convection was slightly delayed with the coarser grid spacing. In contrast with the 1.5-km and 4-km runs, the 12-km run lacks organized convection (Birch et al. 2014a; Pearson et al. 2014) and cold pools (Marsham et al. 2011, 2013a; Heinold et al. 2013).

A quantitative comparison is given by the frequency of surface wind speed over the Sahara in the runs during the 10-day period (Fig. 3). While the 12-km run distribution drops near 12 m s^{-1}, the 4-km run matches the 1.5-km run and captures the tail of distribution up to 20 m s^{-1}. Convective dust storms contribute most of the tail of distribution (not shown). This further supports that the representation of cold pool outflows is similar in the 4-km and 1.5-km runs. Johnson et al. (2014) also show that the timing and structure of a convective outflow are successfully represented with a 4-km grid spacing. The 4-km run is then the only available run that explicitly represents convection and captures the cold pool outflows during the 60-day period, for which the convective mass flux diagnostics were saved out (Table 1). As observations are sparse over the Sahara, the 4-km run is used as a reference for the parameterization of convective dust storms. It provides robust statistics with a large number (many hundreds) of convective dust storms that develop during the 60-day period.

c. Dust uplift potential

Dust uplift occurs when the friction velocity reaches a threshold that depends on soil properties such as mineralogy, roughness elements, and moisture (Marticorena and Bergametti 1995; Shao and Lu 2000). The friction velocity was not saved out in the runs. We therefore estimate dust uplift from the 10-m wind speed, which largely controls the friction velocity. Several authors have directly computed the friction velocity from the 10-m wind speed (e.g., Cakmur et al. 2004; Miller et al. 2008; Ridley et al. 2013; Fiedler et al. 2013). Here we follow Marsham et al. (2011) and compute the dust uplift potential

$$\mathrm{DUP} = \nu U_{10}^3 \left(1 + \frac{U_t}{U_{10}}\right)\left(1 - \frac{U_t^2}{U_{10}^2}\right), \tag{1}$$

with ν the fraction of bare soil, U_{10} the 10-m wind speed, and $U_t = 7$ m s^{-1} a fixed threshold for dust uplift. The DUP isolates the atmospheric control from the soil control on dust uplift, and thus can easily be computed offline without a full model for dust emission. Heinold et al. (2013) showed that DUP is largely consistent with both the diurnal cycle and the geographical distribution of dust emission fluxes from such a full model. Marsham et al. (2013b) further showed that DUP correlates with observed dust over the central Sahara.

The geographical distribution of DUP exhibits similar patterns in the 4-km and 12-km runs (Fig. 4). Highest DUP is found over the Saharan heat low region from eastern Mauritania to northern Mali (18-22°N, 12-2°W) and over the Bodélé Depression in northern Chad (16-20°N, 15-20°E). High DUP is found over southwestern Algeria (24-27°N, 5-0°W), where it is related to the flow around the Hoggar Mountains (Birch et al. 2012), and over northeastern Niger (20-24°N, 10-18°E). High DUP is also found along the coast of Mauritania and Western Sahara, where the Atlantic inflow produces strong winds during the afternoon and evening (Grams et al. 2010).

Apart from the Atlantic coast, the areas of high DUP coincide with the areas of highest fraction of bare soil (Fig. 1b). However, the pattern of bare soil does not directly impact the pattern of DUP: omitting v in Eq. 1 produces a similar pattern of DUP (not shown). Instead, the low roughness length over bare soil (Fig. 1c) allows for strong winds that result in high DUP (Fig. 4). The sharp border in DUP along the Sahel (near 16°N in Fig. 4) matches the strong gradient in roughness length (Fig. 1c). The roughness length increases over mountain ranges, because it accounts for subgrid orography (Fig. 1a). High roughness length prevents strong winds and DUP over the Tibesti (19-24°N, 16-20°E) and Hoggar (22-27°N, 3-13°E) mountain ranges (Fig. 4).

Figure 5 displays the diurnal cycle of DUP over the Sahara. A strong peak occurs in the morning and is attributed to the breakdown of the nocturnal low-level jet (Knippertz 2008; Fiedler et al. 2013). The 12-km run underestimates the amplitude of the peak compared to the 4-km run (Fig. 5). In contrast, the 12-km run overestimated the amplitude of the peak during the 10-day period, due to a deeper Saharan heat low, and thus a stronger pressure gradient compared to the 4-km run (Marsham et al. 2013a; Heinold et al. 2013). Here, the 12-km run exhibits a shallower Saharan heat low than the 4-km run (contours in Fig. 4). This demonstrates how sensitive the monsoon circulation is to the time period and representation of convection in a given model (Marsham et al. 2013a). The weaker pressure gradient in the 12-km run results in weaker nocturnal low-level jets and therefore weaker DUP in the morning compared to the 4-km run (Fig. 5). Heinold et al. (2013) showed that low-level jets can form in aged cold pools, such that some of the differences between the two runs may indirectly be related to the lack of organized convection in the 12-km run.

A second, weaker peak in DUP occurs in the afternoon, in both 4-km and 12-km runs (Fig. 5). This peak is attributed to dry convection in the boundary layer, which reaches its peak in the afternoon and which was observed to enhance dust uplift (Chaboureau et al. 2007; Marsham et al. 2008a). DUP then remains high in the evening in the 4-km run, while it drops in the 12-km run.

The weaker DUP in the 12-km run was attributed to the lack of convective dust storms in the evening during the 10-day period (Marsham et al. 2011; Heinold et al. 2013). The contribution of convective dust storms to DUP in the 4-km run is discussed below.

d. Identification of convective dust storms

Convective dust storms need to be identified in the 4-km run, which is used as a reference to calibrate the parameterization. Following Heinold et al. (2013), surface winds are attributed to convective dust storms if they occur within 40 km of a grid point of rapid cooling and strong vertical velocities. These conditions are met at the leading edge of cold pool outflows (see example of cold pool outflow in Section 3a). Additional conditions in potential temperature and wind divergence suggested by Heinold et al. (2013) were found redundant here with the conditions in cooling and vertical velocity, respectively.

A visual inspection of several cold pool outflows in the 4-km run delivered thresholds $\dot{T}_t = -1$ K h^{-1} for temperature tendency and $|w|_t = 0.5$ m s^{-1} for vertical velocity of up- and downdrafts. The 1-h temperature tendency is computed on the 133-m model level and defined as the anomaly with respect to the 5-day average of the diurnal cycle, while the vertical velocity is taken on the 1605-m model level. The choice of 1-h tendency and 5-day average was constrained by the organization of model data, while the choice of model levels was driven by the strongest signature of cold pools in temperature tendency and vertical velocity.

The thresholds are close to those defined by Heinold et al. (2013). Figure 6 shows the diurnal cycle of identified convective dust storms using a range of thresholds $\dot{T}_t$ for temperature tendency and $|w|_t$ for vertical velocity. Regardless of thresholds, DUP from convective dust storms quickly increases from 13 UTC to reach its peak at 18 UTC, consistent with the peak rain at this time (Marsham et al. 2013a; Birch et al. 2014b; Pearson et al. 2014). This contributes to the overall

DUP peak in the afternoon (blue curve in Fig. 5). DUP from convective dust storms then declines until 06 UTC (Fig. 6), when rainfall is low and the strong surface stable layer inhibits cold pool momentum from reaching the surface. A weak peak occurs at 09 UTC, during the breakdown of the nocturnal low-level jet (Fig. 5). This is consistent with cold pool momentum being mixed down to the surface as dry convection erodes the stable layer (Heinold et al. 2013).

Heinold et al. (2013) found low sensitivity to the exact thresholds used. Here, multiplying $\dot{T}_t$ or $|w|_t$ by a factor of 2 increases DUP by 33% and 24%, respectively (red curves in Fig. 6). Dividing $\dot{T}_t$ or $|w|_t$ by a factor of 2 decreases DUP by 42% and 20%, respectively (blue curves in Fig. 6). These results suggest that the uncertainty in the contribution of convective dust storms is on the order of 30%. The uncertainty accounts both for spurious rejection of cold pool outflows and for spurious identification of other processes. While isolated cold pools are distinct, however, their identification is ambiguous when they are embedded in the monsoon flow or evolve into nocturnal low-level jets (Heinold et al. 2013).

3. Conceptual model

In order to address the problem of lacking cold pool dust emission in models with parameterized convection, we now present the conceptual model on the basis of which our parameterization of convective dust storms is built. Section 3a presents the general formulation, while Section 3b shows an illustrative example, which is used to tune the parameterization in Section 3c.

a. Formulation

The parameterization is based on the conceptual model of convective dust storms that is illustrated in Fig. 7: the downdraft mass flux M_{dd} (in kg s^{-1}) spreads out radially in a cylindrical cold pool of radius R and height h. To ensure conservation of mass, the propagation speed of the cold pool must be

$$C = \frac{M_{dd}}{2\pi R h \rho}, \quad (2)$$

with ρ the average density of the cold pool. The conceptual model matches a developing cold pool in the 4-km run: a strong convective downdraft (Figs. 8b,d) spreads out radially in a cylindrical cold pool and creates strong winds at its leading edge (Figs. 8a,c).

When a cold pool propagates as a density current, its radius increases and its propagation speed decreases[1]. In contrast, convective parameterizations assume the quasi equilibrium of subgrid boundary-layer processes (Bechtold et al. 2014). A parameterization of propagating, subgrid cold pools therefore requires the complete coupling with the parameterization of subgrid convection (Grandpeix and Lafore 2010). Such a coupling is beyond the scope of our work. We rather base our parameterization on a single, static cold pool of representative size (with sensitivity to assumptions of size tested in Section 3c). The conceptual model is therefore independent of the model time step if applied online, or of the temporal sampling of model output if applied offline.

Surface friction lifts the leading edge of a density current, which forms a "nose" (Simpson 1999). The developing cold pool in the 4-km run exhibits such a nose with strongest wind at height $z_{max} \approx$ 100 m (Fig. 8c). Below z_{max}, turbulence mixes the surface layer. We assume the surface layer has constant potential temperature, i.e., neutral stability, and that below z_{max} the radial wind speed follows a logarithmic profile

$$U_r(z) = \frac{u^*}{\kappa} \ln(z_{max}/z_0), \quad (3)$$

with z the height above ground, u^* the friction velocity, $\kappa = 0.41$ the von Karman constant, and z_0 the roughness length. Above z_{max}, the radial wind speed decreases with height (Fig. 8c). While the internal flow of the cold pool is directed forward at low levels, it is directed backward closer to

[1]The theoretical propagation speed of a cold pool follows $C \propto R^{-1/3} \propto t^{-1/4}$ if the downdraft mass flux is sustained (Parker 1996), and $C \propto R^{-1} \propto t^{-1/2}$ if the downdraft mass flux is stopped at some point (Simpson 1999).

the top levels (Simpson 1999). For simplicity, we assume the radial wind speed decreases linearly with height above z_{max} and vanishes at height h. The thin black arrows illustrate the vertical profile of the radial wind in Fig. 7.

Combining the logarithmic profile below z_{max} and the linear profile above, the maximum radial wind speed at the leading edge must satisfy,

$$U_r(z_{max}) = \alpha C \tag{4}$$

at height z_{max}, with

$$\alpha = h \left(z_{max} \frac{\ln(z_{max}/z_0) - 1}{\ln(z_{max}/z_0)} + \frac{1}{2}(h - z_{max}) \right)^{-1} \tag{5}$$

to ensure conservation of mass. With typical values $z_{max} = 100$ m and $z_0 = 10^{-3}$ m, α increases from $\alpha \approx 1.1$ for $h = z_{max}$ to $\alpha = 2$ for $h \gg z_{max}$; a height $h = 240$ m delivers the value $\alpha = 1.5$ that was observed in thunderstorm outflows (Goff 1976).

Within the cold pool, we assume M_{dd} to be homogeneous. To ensure conservation of mass, the radial wind speed must read

$$U_r(r) = \frac{r}{R} U_r(R), \tag{6}$$

with r the distance from the center of the cold pool (thin black arrows in Fig. 7). Based on observations of strong downdrafts, Holmes and Oliver (2000) also used Eq. 6 to describe the wind speed for $r < R$. In addition, they suggested an empirical model of the form

$$U_r(r) = e^{-\left(\frac{r-R}{R_0}\right)^2} U_r(R) \tag{7}$$

for $r > R$, with $R_0 \approx 0.5R$ a radial length scale. We apply this empirical model to account for the smooth decrease in wind speed beyond the leading edge of the cold pool (Figs. 8a,c).

The developing cold pool in the 4-km run exhibits asymmetric wind speeds (Figs. 8a,c), because the downdraft transports horizontal momentum from higher levels (Figs. 8b,d). Following Parker

(1996), we write the steering speed of the cold pool,

$$C_{st} = 0.65 U_{env}, \tag{8}$$

where U_{env} is the environmental steering wind. The relevant layer for U_{env} is where the downdraft originates from, and not where it spreads out (Fig. 7). We assume that the steering wind within the cold pool (gray arrows) follows the vertical profile of the radial wind (black arrows). The maximum steering wind therefore reads

$$U_{st}(z_{max}) = \alpha C_{st} \tag{9}$$

at height z_{max}, with α given by Eq. 5.

Following Holmes and Oliver (2000), the total wind is obtained from the vector addition of radial and steering wind,

$$U_{tot}(\mathbf{r}) = \frac{\mathbf{r}}{R} U_r(r) + \mathbf{U}_{st}. \tag{10}$$

The conceptual model does not explicitly account for the vertical wind shear. The wind shear sustains cold pools in organized convective systems (Rotunno et al. 1988) but does not impact the propagation of a cold pool as a density current (Parker 1996).

b. Illustration

Equations 2 to 10 describe the conceptual model. In the following, we apply them to the developing cold pool in the 4-km run (Fig. 8). The downdraft mass flux is computed from the vertical velocity w_{dd} of downdrafts as

$$M_{dd} = \int_A \rho w_{dd} dA, \tag{11}$$

with A the area of the cold pool. The downdraft mass flux reaches its peak $M_{dd} = 1.5 \times 10^9$ kg s^{-1} on the 1605-m model level (Fig. 8b). The average environmental wind within the cold pool reaches

$U_{env} = 4.5$ m s^{-1} and blows west-southwestward on the same model level. A visual estimate gives parameters $R = 20$ km, $R_0 = 0.33R$ (Fig. 8a), $h = 2$ km, and $z_{max} = 100$ m (Fig. 8c); additional parameters are $\rho = 1$ kg m^{-3} and $z_0 = 5 \times 10^{-3}$ m in the model run.

Given the estimated parameters, the conceptual model yields $C = 6.0$ m s^{-1} (Eq. 2), $\alpha = 1.9$ (Eq. 5), $U_r(z_{max}) = 11.5$ m s^{-1} (Eq. 4), and $U_{st}(z_{max}) = 5.7$ m s^{-1} (Eqs. 8 and 9). The radial wind at height z_{max} is computed from Eqs. 6 and 7, then the total wind at height z_{max} is computed from Eq. 10. Finally, the total wind is extrapolated to $z = 10$ m from Eq. 3. Alternatively, the friction velocity can be computed from the total wind in Eq. 3. The total wind is set to vanish at distance $r = R + R_0$ from the center, to avoid the environmental wind extending outside of the cold pool.

Figure 9 illustrates the resulting wind field. The conceptual model captures the asymmetric structure of the cold pool outflow and its magnitude in the 4-km run (Figs. 8a,c). The exact intensity of surface winds can be obtained by tuning the parameters carefully. The strong wind speed along the downdraft at the center of the cold pool (Figs. 8c,d) is lacking in the conceptual model (Fig. 9b), but it does not affect the surface wind. New up- and downdrafts at the leading edge of the cold pool (Figs. 8b,d) are also lacking as expected in the conceptual model, but they play a minor role during the early development of the cold pool.

The 4-km run exhibits variability in the structure of cold pool outflows (Fig. 2f). The conceptual model does not account for fine-scale processes that impact the development of cold pools (e.g., surface inhomogeneities, Lothon et al. 2011). However, the crescent shape of surface winds (Fig. 9) matches the typical structure of cold pool outflows in the 4-km run (Fig. 2f). This suggests that the simple assumptions of the conceptual model (Fig. 7) deliver a realistic, albeit idealized, representation of cold pools outflows.

c. Tuning

The downdraft mass flux computed from the vertical velocity of downdrafts (Eq. 11) reaches $M_{dd} = 1.5 \times 10^9$ kg s^{-1} in the developing cold pool of the 4-km run (Fig. 8). In contrast, the downdraft mass flux diagnostic computed in the convective parameterization scheme barely reaches 1.5 $\times$ 10^7 kg s^{-1} over the Sahara in the 12-km run (Fig. 10a). Two reasons explain this difference in magnitude. Firstly, the radius of parameterized convective cells in the 12-km run must be on the order of one kilometer to remain of subgrid size, while the radius of the developing cold pool in the 4-km run reaches $R = 20$ km. Secondly, the downdraft mass flux of the convection scheme is typically too weak, due to the lack of explicit representation of subgrid variability. In particular, a more intense downdraft mass flux would over-stabilize the lower layers (Ben Shipway 2014, UK Met Office, personal communication). Cakmur et al. (2004) scaled the downdraft mass flux of the convection scheme with an empirical constant $\beta = 10$ to compute subgrid wind for dust uplift. Following Cakmur et al. (2004), we scale M_{dd} with an arbitrary factor $f = 10$ in the conceptual model, unless stated otherwise.

Several parameters control the wind speed in the conceptual model: the radius of cold pools R (Eq. 2), the height of cold pools h (Eqs. 2 and 5), the height of maximum winds z_{max} (Eqs. 3 and 5), and the radial length scale R_0 (Eq. 7). We constrain the geometry of cold pool outflows to reduce the number of free parameters to one: based on the developing cold pool in the 4-km run (Fig. 8), we set $h/R = 0.1$, $z_{max} = 100$ m, and $R_0/R = 0.33$. The parameterization now depends on R only. Using a different constraint on the geometry of the cold pool requires a different tuning of R but weakly impacts the resulting DUP.

The free parameter R is tuned for the average parameterized DUP to match the average reference DUP (the calibration area is discussed in Section 4). The parameterized DUP is computed from the parameterized subgrid wind and averaged over the grid cells in the 12-km run, while the reference DUP is computed from the model wind attributed to convective dust storms in the 4-km run. Using a trial-and-error method, the best match of the parameterized DUP with the reference DUP is found for a radius of cold pools $R = 2.0$ km. The constraint on the geometry of cold pools gives a height $h = 0.2$ km. Parameterized downdrafts of subgrid scale spread out in cold pools of subgrid scale as expected. Their radius corresponds to the typical radius of microbursts (Fujita 1985).

An additional, hidden parameter of the conceptual model is the height at which the environmental wind U_{env} is taken. Figure 10b illustrates the distribution of U_{env} over the Sahara at different model levels in the 12-km run. The distribution of U_{env} is computed where M_{dd} is positive only, i.e. where the parameterization will be applied. Increasing the height between 2210 and 4210 m quickly shifts the distribution to stronger U_{env}. The distribution is more stable below and above this range of heights (not shown). This shows that the chosen level strongly impacts the value of U_{env} in the parameterization. However, the chosen level weakly impacts the surface wind: a typical U_{env} = 5 m s^{-1} (Fig. 10b) yields a steering speed of the cold pool C_{st} = 3 m s^{-1} (Eq. 8). In comparison, a typical $M_{dd} = 5 \times 10^6$ kg s^{-1} (Fig. 10a) scaled by $f = 10$ yields a propagation speed of the cold pool C = 20 m s^{-1} (Eq. 2). The height at which U_{env} is taken is therefore not expected to strongly affect the DUP overall, but may impact DUP locally if high U_{env} combines with low M_{dd}. Here the 3130-m level was chosen as a compromise between weaker and stronger environmental winds (Fig. 10b).

4. Space and time distribution of convective dust storms

The DUP from convective dust storms is first discussed in the 4-km run. Identified convective dust storms produce DUP over the southern Sahara mainly (around 18°N, Fig. 11a), where the monsoon flow brings the necessary moisture to trigger convection. Highest DUP is found over the Saharan heat low from eastern Mauritania to northern Mali, as for the total DUP (Fig. 4a). In contrast, low DUP is found over the Bodélé Depression in northern Chad and over southwestern Algeria (Fig. 11a), consistent with known wind sources that are not related to cold pools in these regions (Washington and Todd 2005; Birch et al. 2012). Local concentrations of DUP are found over southern Algeria and northeastern Niger, in the vicinity of mountain ranges (Fig. 4a), consistent with orographic triggering of moist convection.

The parameterization of convective dust storms in the 12-km run succeeds at producing high DUP over the southern Sahara (around 18°N, Fig. 11b). The parameterized DUP is shifted eastward compared to the DUP from identified convective dust storms in the 4-km run (Fig. 11a). The eastward shift in the location of DUP is due to the eastward shift in the location of precipitation between the 12-km and the 4-km runs (contours in Fig. 11). The location of precipitation is coupled with the pressure gradient of the Saharan heat low (contours in Fig. 4) through the dynamics of the monsoon (Marsham et al. 2013a; Birch et al. 2014b). The parameterized DUP further lacks local concentrations in the vicinity of mountain ranges compared to the 4-km run (Fig. 11), because of the relative lack of moist convection in the vicinity of mountain ranges in the 12-km run.

Although most of DUP over the Sahel south of 16°N is attributed to convective dust storms in the 4-km run, it remains small compared to DUP over the Sahara (Figs. 4a and 11a). The parameterized DUP extends farther south across the Sahel (Fig. 11). This appears more realistic than the sharp border in the 4-km run, as convective dust storms have been observed along a transect around 14°N at the beginning of the monsoon season (Marticorena et al. 2010). The high roughness length over the Sahel (Fig. 1c) prevents strong winds in the model runs; it is possibly too high for the beginning of the monsoon season, when the vegetation has not yet developed.

High DUP is also attributed to convective dust storms along the coast in the 4-km run (Fig. 11a). The Atlantic inflow is identified as a cold pool outflow, because its front propagates as a density current (Grams et al. 2010). However, the Atlantic inflow does not result from convection; it is therefore excluded from the calibration area (boxes in Fig. 11). The northern and eastern margins of the nested 4-km domain are also excluded from the calibration area to avoid contamination from the lateral boundaries. The calibration area also excludes the area south of 15°N, because the reference 4-km run may underestimate DUP over the Sahel.

As seen in Fig. 6, DUP from convective dust storms exhibits a strong diurnal cycle in the 4-km run (Fig. 12, blue curve). Convective dust storms contribute 27 % of the total DUP from 13 UTC to 06 UTC and 16 % of the total daily DUP, over the calibration area displayed in Fig. 11a. The parameterized DUP succeeds at exhibiting a strong diurnal cycle (Fig. 12, red curve). As expected, however, the peak of parameterized DUP occurs at 12 UTC instead of 18 UTC in the 4-km run, because convection is triggered too early in the 12-km run (Marsham et al. 2013a; Birch et al. 2014b; Pearson et al. 2014). The parameterized DUP then decreases too quickly after the peak since the moist convection is too short-lived in the 12-km run. As the parameterization is calibrated with the daily DUP, the amplitude of the peak is overestimated compared to the 4-km run (Fig. 12). Therefore, the main biases in timing and amplitude of DUP are due to biases in the convective parameterization scheme, and not to the parameterization of convective dust storms.

5. Conclusion

We suggest a parameterization of convective dust storms for models with mass-flux convection schemes. The parameterization is based on a set of Unified Model runs over West Africa for June and July 2006. It is applied to a convection-parameterized run with 12-km grid spacing, which lacks convective dust storms. A convection-permitting run with 4-km grid spacing captures the dynamics of convective dust storms and is used as a reference for validation and tuning.

Our conceptual model of convective dust storms follows simple assumptions (Fig. 7). The downdraft mass flux – a known value from the convective parameterization scheme – spreads out radially in a static, cylindrical cold pool. The resulting radial wind adds to the steering wind of the downdraft. Together, they follow a logarithmic profile below the "nose" of the cold pool, and decrease linearly with height above. The conceptual model reproduces the structure and magnitude of wind speed for a developing cold pool in the reference run.

The parameterization produces a distribution of subgrid wind in each grid cell of the 12-km run. It is calibrated to match the integrated dust generating winds (dust uplift potential, DUP) from identified convective dust storms over the Sahara in the reference run. The geometry of the cold pools is constrained in the parameterization, based on a developing cold pool in the reference run. The only free parameter is the radius of the cold pools, which is taken as constant for the whole domain and the whole period. The calibration delivers a radius of 2.0 km, consistent with the subgrid downdraft mass fluxes producing subgrid cold pools.

The parameterization of convective dust storms successfully produces high DUP over the southern Sahara. The parameterized DUP is more spread out than in the reference run: it lacks local concentrations over the central Sahara and extends farther east over the southern Sahara. Over the Sahel, the parameterized DUP extends farther south and appears more realistic than the reference run, which shows a sharp border at 16°N. The parameterization of convective dust storms also successfully produces a strong diurnal cycle of DUP. The parameterized DUP peaks 6-h earlier and reaches higher amplitude than in the reference run.

Compared to the reference run, differences in the geographical distribution of parameterized convective dust storms originate from differences in the monsoon flow between the model runs. Differences in the timing of convective dust storms also originate from differences in the timing of convection between the model runs. The dynamics of the West African monsoon (e.g., Marsham et al. 2013a) and the diurnal cycle of tropical convection (e.g., Bechtold et al. 2014) are know issues for modeling and are topics of active research. These issues are separate from the lack of convective dust storms addressed here and solving them is beyond the scope of this paper.

The results suggest that the new parameterization allows a useful estimate of dust uplift due to convective dust storms. The distribution and timing of DUP are weakly sensitive to the parameters of the conceptual model, if the radius of cold pools is carefully calibrated. The main uncertainty originates from the calibration, which is sensitive to the model resolution, the chosen domain and period, the identification of convective dust storms, and the estimate of dust uplift in the reference run. The uncertainty, however, remains small compared to large uncertainties in the estimation of dust uplift from models and observations (Huneeus et al. 2011).

As the parameterization produces a distribution of subgrid wind, it can be implemented in a full model for dust emission. If required, the parameterization can alternatively produce a distribution of subgrid friction velocity. A more accurate estimate of dust uplift can then be used instead of the simple DUP to tune the parameterization for the full model. The uplifted dust will then be transported beyond the grid cell, mixed, or deposited by the meteorology of the model. Through both wetting of the soil and scavenging, convective precipitation within a column may reduce the efficiency of convective dust storms in that column in a full dust model. To account for the spatial separation between the gust front and the precipitation in a realistic convective dust storm, the best approach may be to switch off the soil moisture effect and the scavenging during time steps when the parameterization is activated. A more detailed investigation of this effect is left for future applications in a fully online coupled system.

Further work is needed to test the sensitivity of the parameterization to different periods, grid spacings, and models. Current parameters of the conceptual model may vary: e.g., the radius of cold pools, which is expected to increase with increasing grid spacing. Parameterized convective dust storms would have more realistic dimensions with grid spacings on the order of 100 km. Additional parameters may be included in the conceptual model: e.g., the vertical wind shear, which is crucial for the organization of convection (Rotunno et al. 1988). If proven robust, the parameterization will substantially improve the representation of a key ingredient to dust emission and allow studies of the impact of convective dust storms in large-scale weather and climate models that use mass-flux convection schemes.

Acknowledgments. We thank Françoise Guichard and her colleagues at the CNRM in Toulouse for valuable discussions about the parameterization of convective dust storms, and Adrian Lock at the UK Met Office in Exeter for helpful explanations about the boundary layer in the Unified Model. We also thank three anonymous reviewers for their useful comments on an earlier version of this manuscript. This work was funded by ERC grant 257543 "Desert Storms". The Cascade project was funded by NERC grant NE/E003826.

References

Allen, C. J., R. Washington, and S. Engelstaedter, 2013: Dust emission and transport mechanisms in the central Sahara: Fennec ground-based observations from Bordj Badji Mokhtar, June 2011. *J. Geophys. Res. Atmos.*, **118 (12)**, 6212–6232, doi:10.1002/jgrd.50534.

Bechtold, P., N. Semane, P. Lopez, J.-P. Chaboureau, A. Beljaars, and N. Bormann, 2014: Representing equilibrium and nonequilibrium convection in large-scale models. *J. Atmos. Sci.*, **71 (2)**, 734–753, doi:10.1175/JAS-D-13-0163.1.

Birch, C. E., J. H. Marsham, D. J. Parker, and C. M. Taylor, 2014a: The scale dependence and structure of convergence fields preceding the initiation of deep convection. *Geophys. Res. Lett.*, **41 (13)**, 4769–4776, doi:10.1002/2014GL060493.

Birch, C. E., D. J. Parker, J. H. Marsham, D. Copsey, and L. Garcia-Carreras, 2014b: A seamless assessment of the role of convection in the water cycle of the West African Monsoon. *J. Geophys. Res. Atmos.*, **119 (6)**, 2890–2912, doi:10.1002/2013JD020887.

Birch, C. E., D. J. Parker, J. H. Marsham, and G. M. Devine, 2012: The effect of orography and surface albedo on stratification in the summertime Saharan boundary layer: Dynamics and implications for dust transport. *J. Geophys. Res. Atmos.*, **117 (D5)**, n/a–n/a, doi:10.1029/2011JD015965.

Bou Karam, D., C. Flamant, P. Knippertz, O. Reitebuch, J. Pelon, M. Chong, and A. Dabas, 2008: Dust emissions over the Sahel associated with the West African monsoon intertropical discontinuity region: A representative case-study. *Quart. J. Roy. Meteor. Soc.*, **134 (632)**, 621–634, doi:10.1002/qj.244.

Byers, H. R., 1949: Structure and Dynamics of the Thunderstorm. *Science*, **110 (2856)**, 291–294, doi:10.1126/science.110.2856.291.

Cakmur, R., R. Miller, and O. Torres, 2004: Incorporating the effect of small-scale circulations upon dust emission in an atmospheric general circulation model. *J. Geophys. Res. Atmos. (1984–2012)*, **109 (D7)**, doi:10.1029/2003JD004067.

Chaboureau, J.-P., P. Tulet, and C. Mari, 2007: Diurnal cycle of dust and cirrus over West Africa as seen from Meteosat Second Generation satellite and a regional forecast model. *Geophys. Res. Lett.*, **34 (2)**, n/a–n/a, doi:10.1029/2006GL027771.

Dai, A., 2006: Precipitation characteristics in eighteen coupled climate models. *J. Climate*, **19 (18)**, 4605–4630, doi:10.1175/JCLI3884.1.

Fiedler, S., K. Schepanski, B. Heinold, P. Knippertz, and I. Tegen, 2013: Climatology of nocturnal low-level jets over North Africa and implications for modeling mineral dust emission. *J. Geophys. Res. Atmos.*, **118 (12)**, 6100–6121, doi:10.1002/jgrd.50394.

Flamant, C., J.-P. Chaboureau, D. J. Parker, C. M. Taylor, J.-P. Cammas, O. Bock, F. Timouk, and J. Pelon, 2007: Airborne observations of the impact of a convective system on the planetary boundary layer thermodynamics and aerosol distribution in the inter-tropical discontinuity region of the West African Monsoon. *Quart. J. Roy. Meteor. Soc.*, **133 (626)**, 1175–1189, doi: 10.1002/qj.97.

Fujita, T., 1985: *The downburst: microburst and macroburst : report of projects NIMROD and JAWS*. SMRP research paper, Satellite and Mesometeorology Research Project, Dept. of the Geophysical Sciences, University of Chicago.

Garcia-Carreras, L., and Coauthors, 2013: The impact of convective cold pool outflows on model biases in the Sahara. *Geophys. Res. Lett.*, **40 (8)**, 1647–1652, doi:10.1002/grl.50239.

Goff, R. C., 1976: Vertical structure of thunderstorm outflows. *Mon. Wea. Rev.*, **104 (11)**, 1429–1440, doi:10.1175/1520-0493(1976)104⟨1429:VSOTO⟩2.0.CO;2.

Grams, C. M., S. C. Jones, J. H. Marsham, D. J. Parker, J. M. Haywood, and V. Heuveline, 2010: The Atlantic inflow to the Saharan heat low: observations and modelling. *Quart. J. Roy. Meteor. Soc.*, **136 (S1)**, 125–140, doi:10.1002/qj.429.

Grandpeix, J.-Y., and J.-P. Lafore, 2010: A density current parameterization coupled with Emanuel's convection scheme. Part I: The models. *J. Atmos. Sci.*, **67 (4)**, 881–897, doi: 10.1175/2009JAS3044.1.

Gregory, D., and P. Rowntree, 1990: A mass flux convection scheme with representation of cloud ensemble characteristics and stability-dependent closure. *Mon. Wea. Rev.*, **118 (7)**, 1483–1506, doi:10.1175/1520-0493(1990)118.

Heinold, B., P. Knippertz, J. Marsham, S. Fiedler, N. Dixon, K. Schepanski, B. Laurent, and I. Tegen, 2013: The role of deep convection and nocturnal low-level jets for dust emission in summertime West Africa: Estimates from convection-permitting simulations. *J. Geophys. Res. Atmos.*, **118 (10)**, 4385–4400, doi:10.1002/jgrd.50402.

Holmes, J., and S. Oliver, 2000: An empirical model of a downburst . *Engineering Structures*, **22 (9)**, 1167–1172, doi:10.1016/S0141-0296(99)00058-9.

Hourdin, F., M. Gueye, B. Diallo, J.-L. Dufresne, L. Menut, B. Marticoréna, G. Siour, and F. Guichard, 2014: Parametrization of convective transport in the boundary layer and its impact on the representation of diurnal cycle of wind and dust emissions. *Atmos. Chem. Phys. Discuss.*, **14 (19)**, 27 425–27 458, doi:10.5194/acpd-14-27425-2014.

Houze, R. A., 2004: Mesoscale convective systems. *Rev. Geophys.*, **42 (4)**, n/a–n/a, doi:10.1029/2004RG000150.

Huneeus, N., and Coauthors, 2011: Global dust model intercomparison in AeroCom phase I. *Atmos. Chem. Phys.*, **11 (15)**, 7781–7816, doi:10.5194/acp-11-7781-2011.

Johnson, R. H., R. S. Schumacher, J. H. Ruppert Jr, D. T. Lindsey, J. E. Ruthford, and L. Kriederman, 2014: The Role of Convective Outflow in the Waldo Canyon Fire. *Mon. Wea. Rev.*, **(2014)**, doi:10.1175/MWR-D-13-00361.1.

Knippertz, P., 2008: Dust emissions in the West African heat trough–the role of the diurnal cycle and of extratropical disturbances. *Meteorol. Z.*, **17 (5)**, 553–563, doi:10.1127/0941-2948/2008/0315.

Knippertz, P., 2014: Meteorological Aspects of Dust Storms. *Mineral Dust*, P. Knippertz, and J.-B. W. Stuut, Eds., Springer Netherlands, 121–147, doi:10.1007/978-94-017-8978-3_6.

Knippertz, P., C. Deutscher, K. Kandler, T. Müller, O. Schulz, and L. Schütz, 2007: Dust mobilization due to density currents in the Atlas region: Observations from the Saharan Mineral Dust Experiment 2006 field campaign. *J. Geophys. Res. Atmos. (1984–2012)*, **112 (D21)**, doi:10.1029/2007JD008774.

Knippertz, P., and M. C. Todd, 2012: Mineral dust aerosols over the Sahara: Meteorological controls on emission and transport and implications for modeling. *Rev. Geophys.*, **50 (1)**, doi:10.1029/2011RG000362.

Kocha, C., P. Tulet, J.-P. Lafore, and C. Flamant, 2013: The importance of the diurnal cycle of Aerosol Optical Depth in West Africa. *Geophys. Res. Lett.*, **40 (4)**, 785–790, doi:10.1002/grl.50143.

Lothon, M., B. Campistron, M. Chong, F. Couvreux, F. Guichard, C. Rio, and E. Williams, 2011: Life cycle of a mesoscale circular gust front observed by a C-band Doppler radar in West Africa. *Mon. Wea. Rev.*, **139 (5)**, 1370–1388, doi:10.1175/2010MWR3480.1.

Marsham, J. H., N. S. Dixon, L. Garcia-Carreras, G. Lister, D. J. Parker, P. Knippertz, and C. E. Birch, 2013a: The role of moist convection in the West African monsoon system: Insights from continental-scale convection-permitting simulations. *Geophys. Res. Lett.*, **40 (9)**, 1843–1849, doi:10.1002/grl.50347.

Marsham, J. H., C. M. Grams, and B. Mühr, 2009: Photographs of dust uplift from small-scale atmospheric features. *Weather*, **64 (7)**, 180–181, doi:10.1002/wea.390.

Marsham, J. H., P. Knippertz, N. S. Dixon, D. J. Parker, and G. M. S. Lister, 2011: The importance of the representation of deep convection for modeled dust-generating winds over West Africa during summer. *Geophys. Res. Lett.*, **38 (16)**, n/a–n/a, doi:10.1029/2011GL048368.

Marsham, J. H., D. J. Parker, C. M. Grams, B. T. Johnson, W. M. F. Grey, and A. N. Ross, 2008a: Observations of mesoscale and boundary-layer scale circulations affecting dust transport and uplift over the Sahara. *Atmos. Chem. Phys.*, **8 (23)**, 6979–6993, doi:10.5194/acp-8-6979-2008.

Marsham, J. H., D. J. Parker, C. M. Grams, C. M. Taylor, and J. M. Haywood, 2008b: Uplift of Saharan dust south of the intertropical discontinuity. *J. Geophys. Res. Atmos.*, **113 (D21)**, n/a–n/a, doi:10.1029/2008JD009844.

Marsham, J. H., and Coauthors, 2013b: Meteorology and dust in the central Sahara: Observations from Fennec supersite-1 during the June 2011 Intensive Observation Period. *J. Geophys. Res. Atmos.*, **118 (10)**, 4069–4089, doi:10.1002/jgrd.50211.

Marticorena, B., and G. Bergametti, 1995: Modeling the atmospheric dust cycle: 1. Design of a soil-derived dust emission scheme. *J. Geophys. Res. Atmos.*, **100 (D8)**, 16 415–16 430, doi: 10.1029/95JD00690.

Marticorena, B., and Coauthors, 2010: Temporal variability of mineral dust concentrations over West Africa: analyses of a pluriannual monitoring from the AMMA Sahelian Dust Transect. *Atmos. Chem. Phys.*, **10 (18)**, 8899–8915, doi:10.5194/acp-10-8899-2010.

Miller, S. D., A. P. Kuciauskas, M. Liu, Q. Ji, J. S. Reid, D. W. Breed, A. L. Walker, and A. A. Mandoos, 2008: Haboob dust storms of the southern Arabian Peninsula. *J. Geophys. Res. Atmos.*, **113 (D1)**, n/a–n/a, doi:10.1029/2007JD008550.

Nakamura, K., R. Kershaw, and N. Gait, 1996: Prediction of near-surface gusts generated by deep convection. *Meteorol. Appl.*, **3 (2)**, 157–167, doi:10.1002/met.5060030206.

Nikulin, G., and Coauthors, 2012: Precipitation climatology in an ensemble of CORDEX-Africa regional climate simulations. *J. Climate*, **25 (18)**, 6057–6078, doi:10.1175/JCLI-D-11-00375.1.

Parker, D. J., 1996: Cold pools in shear. *Quart. J. Roy. Meteor. Soc.*, **122 (535)**, 1655–1674, doi:10.1002/qj.49712253509.

Pearson, K. J., R. J. Hogan, R. P. Allan, G. M. S. Lister, and C. E. Holloway, 2010: Evaluation of the model representation of the evolution of convective systems using satellite observations of outgoing longwave radiation. *J. Geophys. Res. Atmos.*, **115 (D20)**, D20 206, doi:10.1029/2010JD014265.

Pearson, K. J., G. M. S. Lister, C. E. Birch, R. P. Allan, R. J. Hogan, and S. J. Woolnough, 2014: Modelling the diurnal cycle of tropical convection across the ‘grey zone’. *Quart. J. Roy. Meteor. Soc.*, **140 (679)**, 491–499, doi:10.1002/qj.2145.

Redelsperger, J.-L., F. Guichard, and S. Mondon, 2000: A parameterization of mesoscale enhancement of surface fluxes for large-scale models. *J. Climate*, **13 (2)**, 402–421, doi:10.1175/1520-0442(2000)0132.0.CO;2.

Ridley, D. A., C. L. Heald, J. Pierce, and M. Evans, 2013: Toward resolution-independent dust emissions in global models: Impacts on the seasonal and spatial distribution of dust. *Geophys. Res. Lett.*, **40 (11)**, 2873–2877, doi:10.1002/grl.50409.

Roberts, A. J., and P. Knippertz, 2014: The formation of a large summertime Saharan dust plume: Convective and synoptic-scale analysis. *J. Geophys. Res. Atmos.*, **119 (4)**, 1766–1785, doi:10.1002/2013JD020667.

Rotunno, R., J. B. Klemp, and M. L. Weisman, 1988: A theory for strong, long-lived squall lines. *J. Atmos. Sci.*, **45 (3)**, 463–485, doi:10.1175/1520-0469(1988)045⟨0463:ATFSLL⟩2.0.CO;2.

Shao, Y., and H. Lu, 2000: A simple expression for wind erosion threshold friction velocity. *J. Geophys. Res. Atmos.*, **105 (D17)**, 22 437–22 443, doi:10.1029/2000JD900304.

Simpson, J. E., 1999: *Gravity currents: In the environment and the laboratory*. Cambridge University Press.

Sutton, L. J., 1925: Haboobs. *Quart. J. Roy. Meteor. Soc.*, **51 (213)**, 25–30, doi:10.1002/qj.49705121305.

Walters, D. N., and Coauthors, 2011: The Met Office Unified Model Global Atmosphere 3.0/3.1 and JULES Global Land 3.0/3.1 configurations. *Geosci. Model Dev.*, **4 (4)**, 919–941, doi:10.5194/gmd-4-919-2011.

Washington, R., and M. C. Todd, 2005: Atmospheric controls on mineral dust emission from the Bodélé Depression, Chad: The role of the low level jet. *Geophys. Res. Lett.*, **32 (17)**, n/a–n/a, doi:10.1029/2005GL023597.

Weisman, M. L., W. C. Skamarock, and J. B. Klemp, 1997: The resolution dependence of explicitly modeled convective systems. *Mon. Wea. Rev.*, **125 (4)**, 527–548, doi:10.1175/1520-0493(1997)125⟨0527:TRDOEM⟩2.0.CO;2.

Yang, G.-Y., and J. Slingo, 2001: The diurnal cycle in the tropics. *Mon. Wea. Rev.*, **129 (4)**, 784–801, doi:10.1175/1520-0493(2001)129.

LIST OF TABLES

TABLE 1. Relevant characteristics of the model runs discussed in the text.

Period	Dates	Grid spacing	Vertical levels	Lateral boundaries	Convection	Mass flux diagnostics
10 day	25 July to 3 August	1.5 km	70	4-km run	explicit	
10 day	25 July to 3 August	4 km	70	12-km run	explicit	
10 day	25 July to 3 August	12 km	38	ECMWF analyses	parameterized	not available
60 day	1 June to 30 July	4 km	70	12-km run	explicit	
60 day	1 June to 30 July	12 km	38	ECMWF analyses	parameterized	available

LIST OF FIGURES

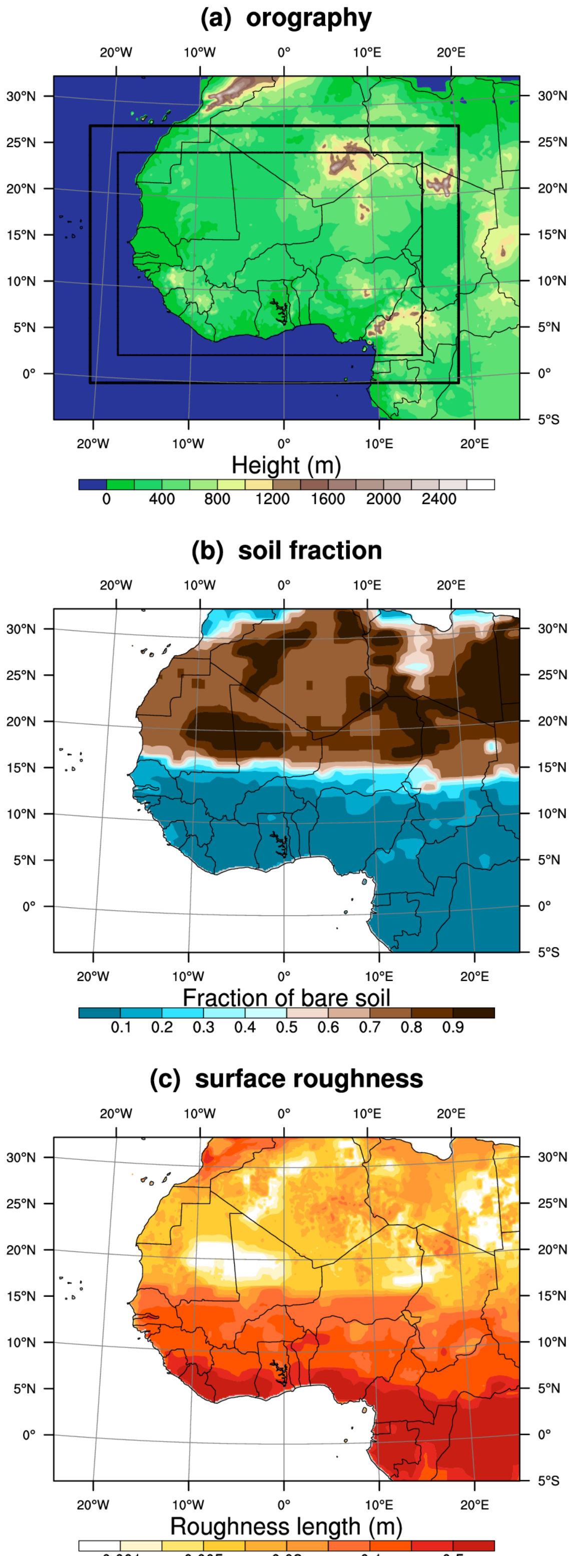

FIG. 1. Orography (a), soil fraction (b), and surface roughness (c) in the 12-km run. The thick and thin boxes in (a) show the nested 4-km and 1.5-km domains, respectively.

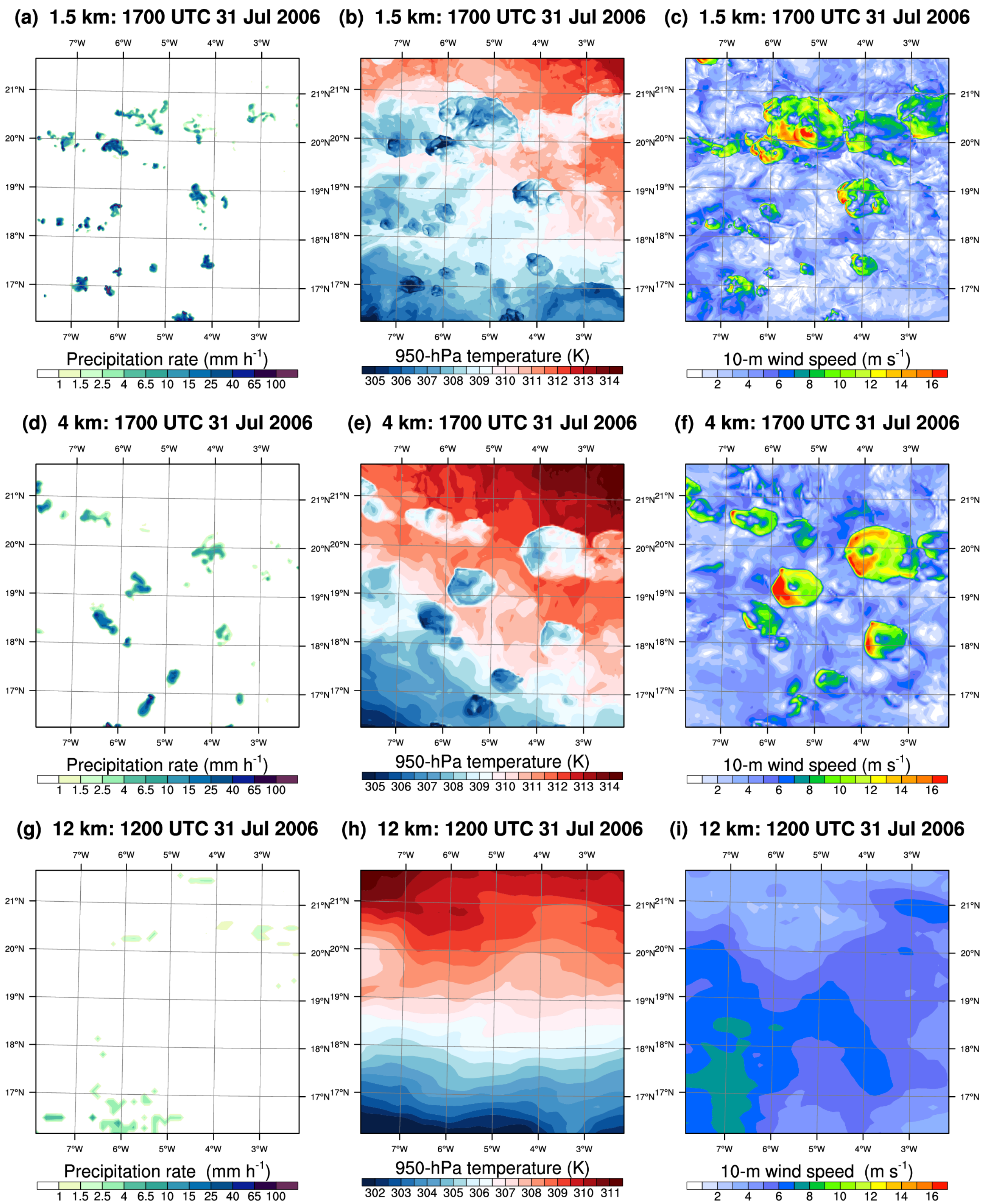

FIG. 2. Example of convection on 31 July 2006 in the 1.5-km (a-c), 4-km (d-f), and 12-km runs (g-i): instantaneous precipitation rate (in mm h^{-1}) (a, d, g), 950-hPa temperature (in K) (b, e, h), and 10-m wind speed (in m s^{-1}) (c, f, i).

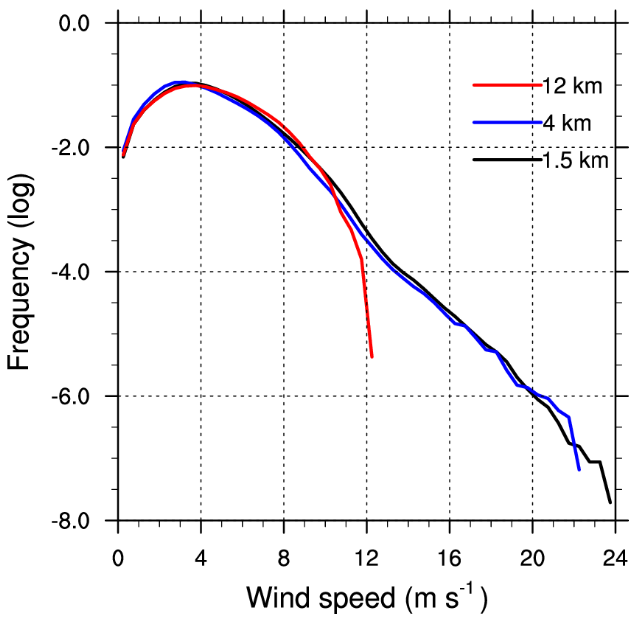

FIG. 3. Probability density function of the 10-m wind speed in the 1.5-km (black curve), 4-km (blue curve), and 12-km runs (red curve). The wind speed is taken from 25 July to 3 August 2006 over the area indicated by the boxes in Fig. 4.

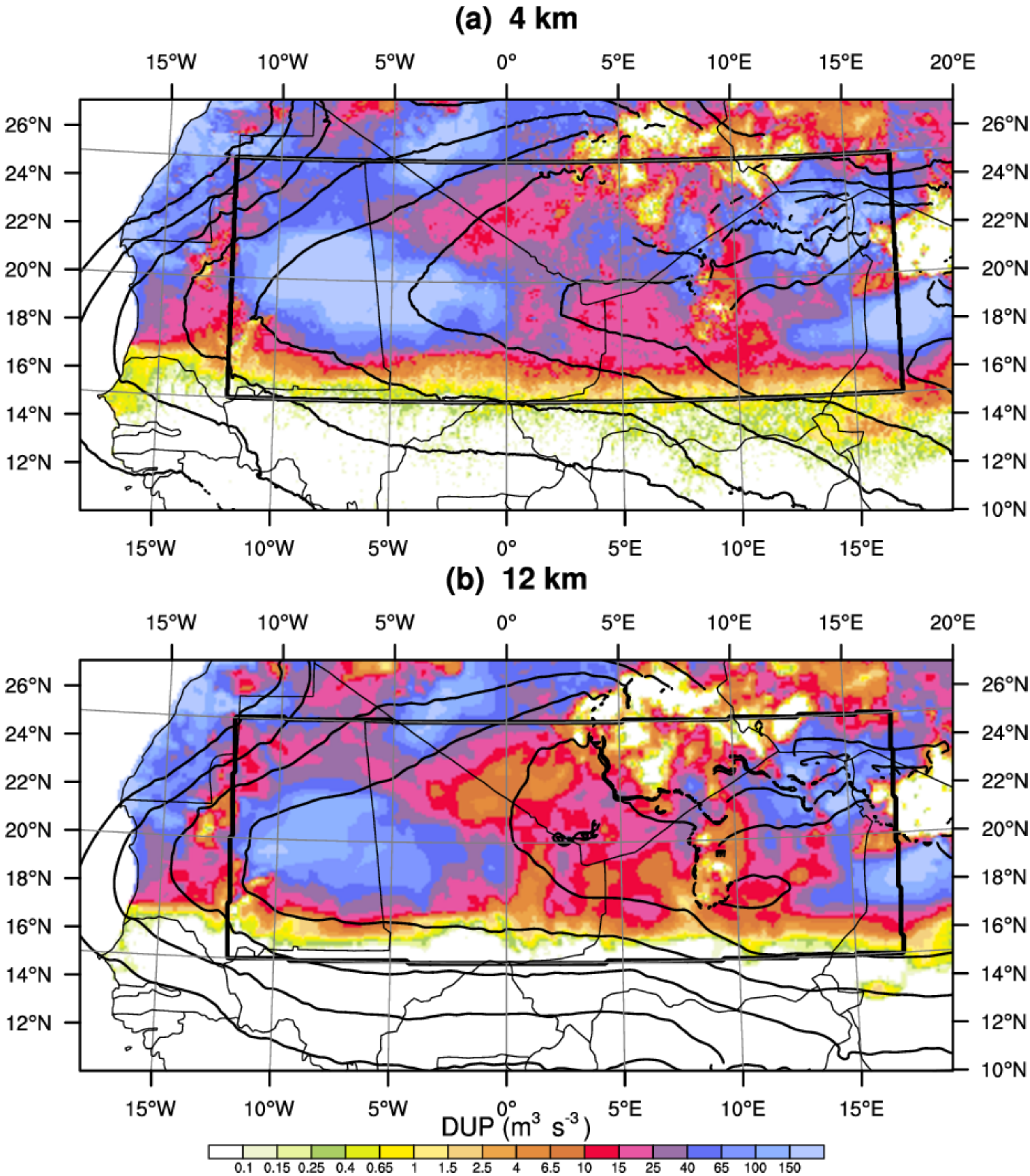

FIG. 4. Dust uplift potential from the model wind (shading, in $m^3\ s^{-3}$) and 925-hPa geopotential height (contours below 790 m, each 5 gpm) averaged from 1 June to 30 July 2006 in the 4-km (a) and 12-km runs (b). The geopotential height is omitted where it lies below the model orography. The displayed area is the northern part of the 4-km domain (Fig. 1). The dust uplift potential is defined in Section 2c. The boxes show the area used to compute the probability density function in Fig. 3 and the diurnal cycles in Figs. 5 and 6.

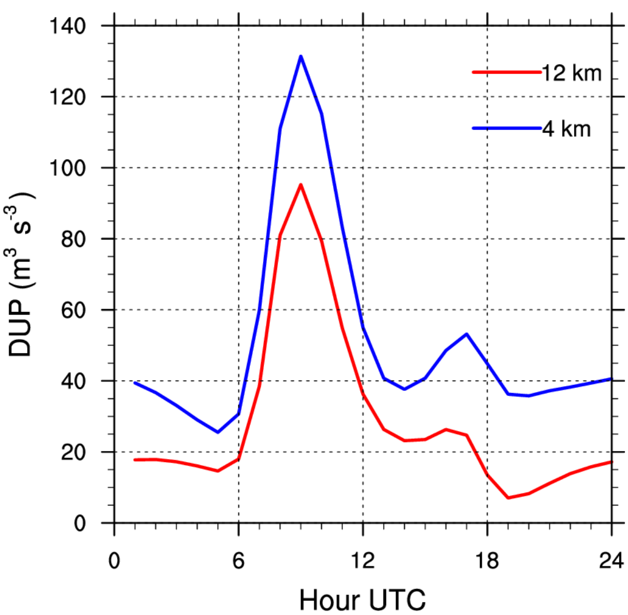

713 FIG. 5. Diurnal cycle of dust uplift potential from the model wind in the 4-km (blue curve) and 12-km runs
714 (red curve). The dust uplift potential is averaged from 1 June to 30 July 2006 over the area displayed in Fig. 4.

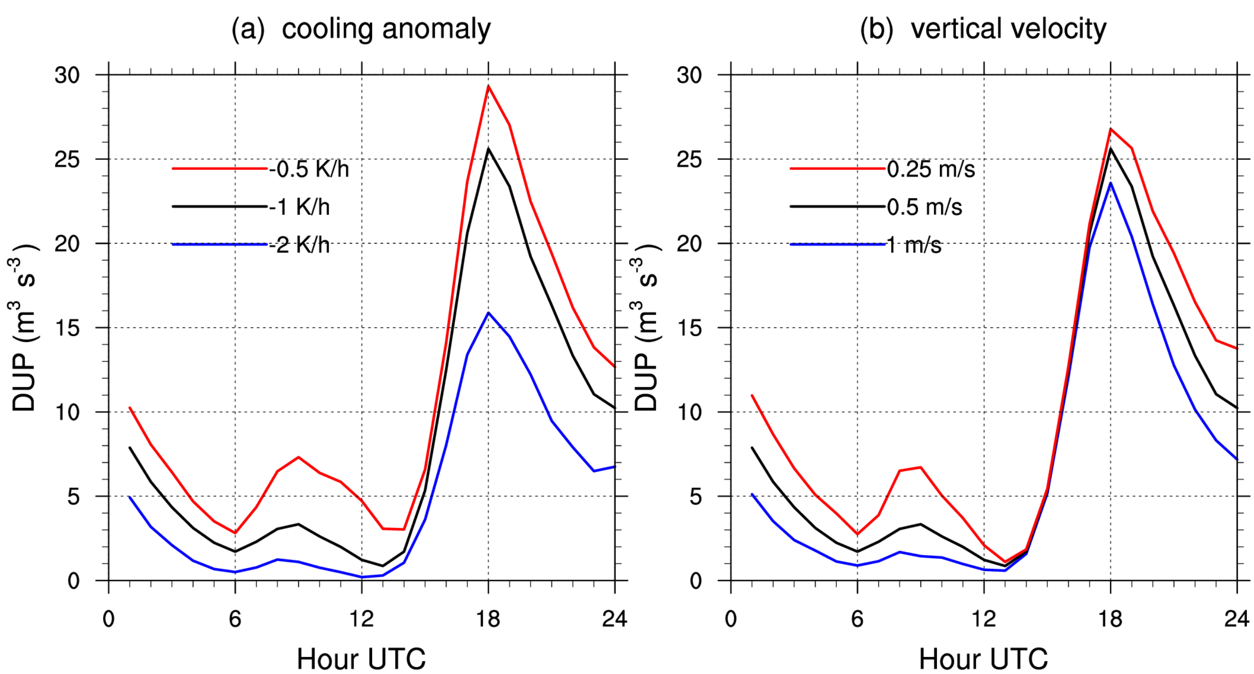

715 FIG. 6. Diurnal cycle of dust uplift potential attributed to convective dust storms in the 4-km run: sensitivity
716 to thresholds in cooling anomaly $\dot{T}_t$ (a) and vertical velocity $|w|_t$ (b). The dust uplift potential is averaged from
717 1 June to 30 July 2006 over the area indicated by the boxes in Fig. 4.

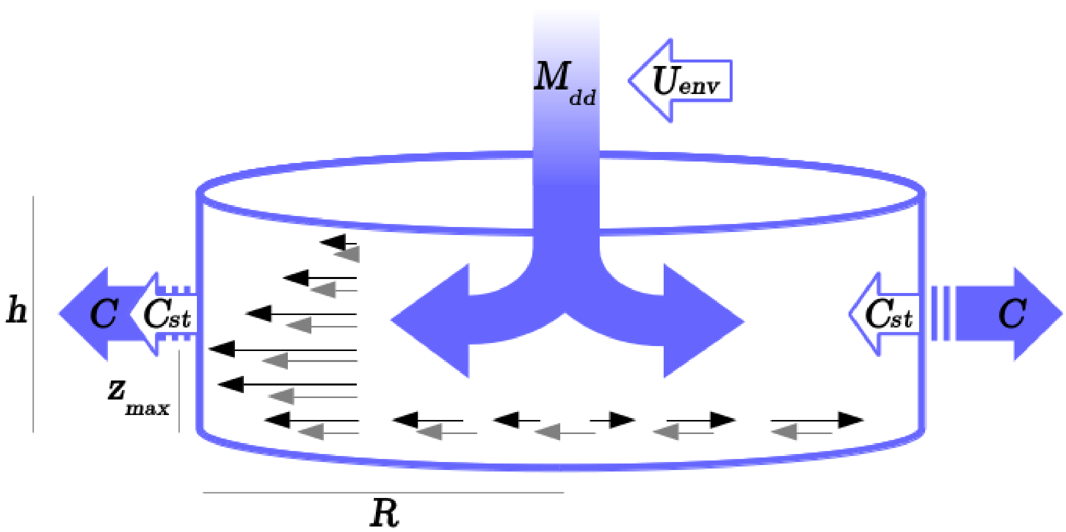

FIG. 7. Schematic of the conceptual model, with M_{dd} the downdraft mass flux, U_{env} the environmental steering wind, C and C_{st} the propagation and steering speeds of the cold pool, respectively, h and R the height and radius of the cold pool, respectively, and z_{max} the height of maximum wind. Thin black and gray arrows illustrate the radial and the steering wind within the cold pool, respectively. See Section 3a for a detailed discussion.

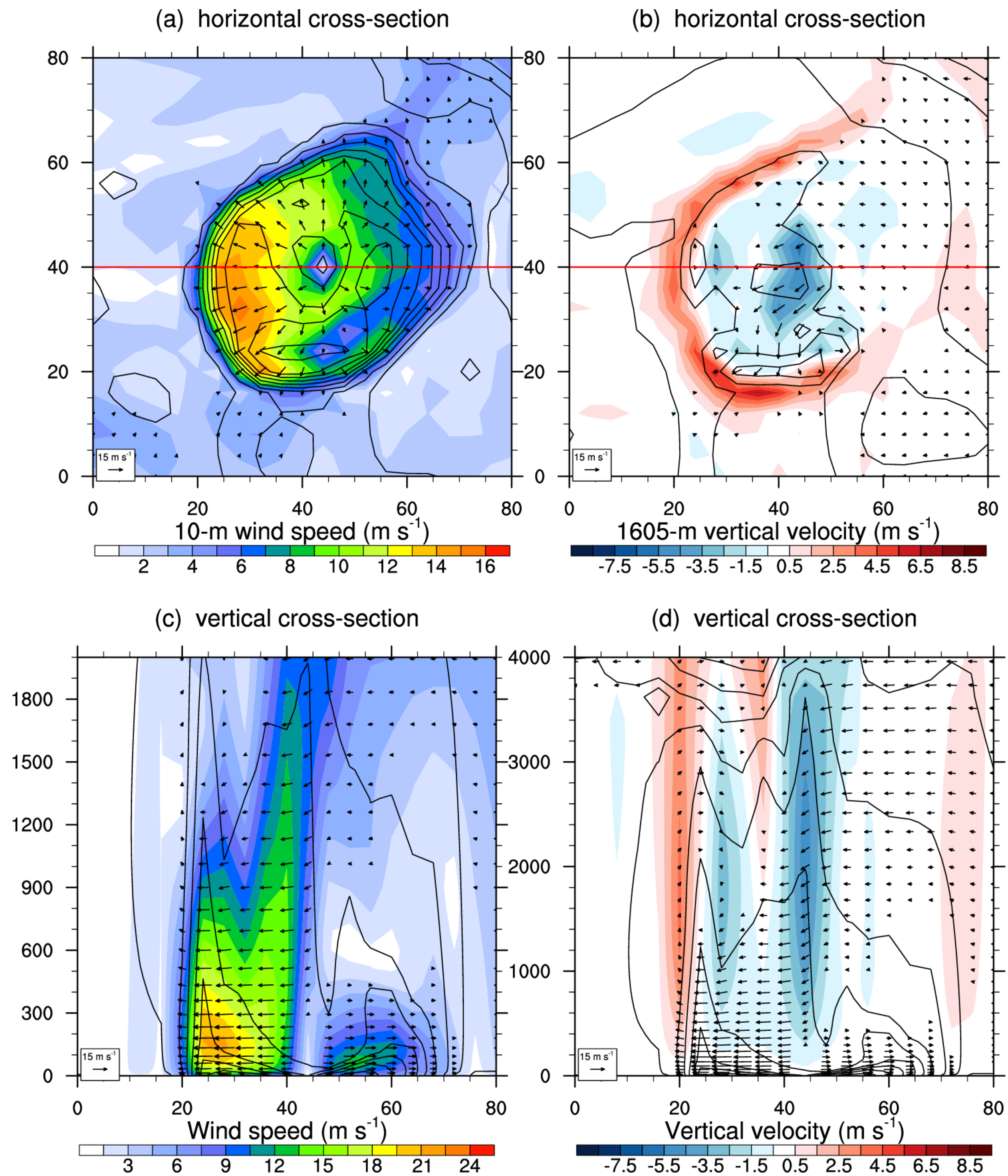

FIG. 8. Example of a cold pool outflow at 1500 UTC 1 July 2006 in the 4-km run: wind speed (shading, in m s^{-1}) (a, c) and vertical velocity (shading, in m s^{-1}) (b, d), in horizontal (a, b) and vertical cross-sections (c, d), showing the section-parallel wind (vectors above 3 m s^{-1} according to the scale) and potential temperature (contours every 1 K) in the cross-sections. Horizontal scales are in km and vertical scales in m. The red lines in (a, b) show the trace of (c, d).

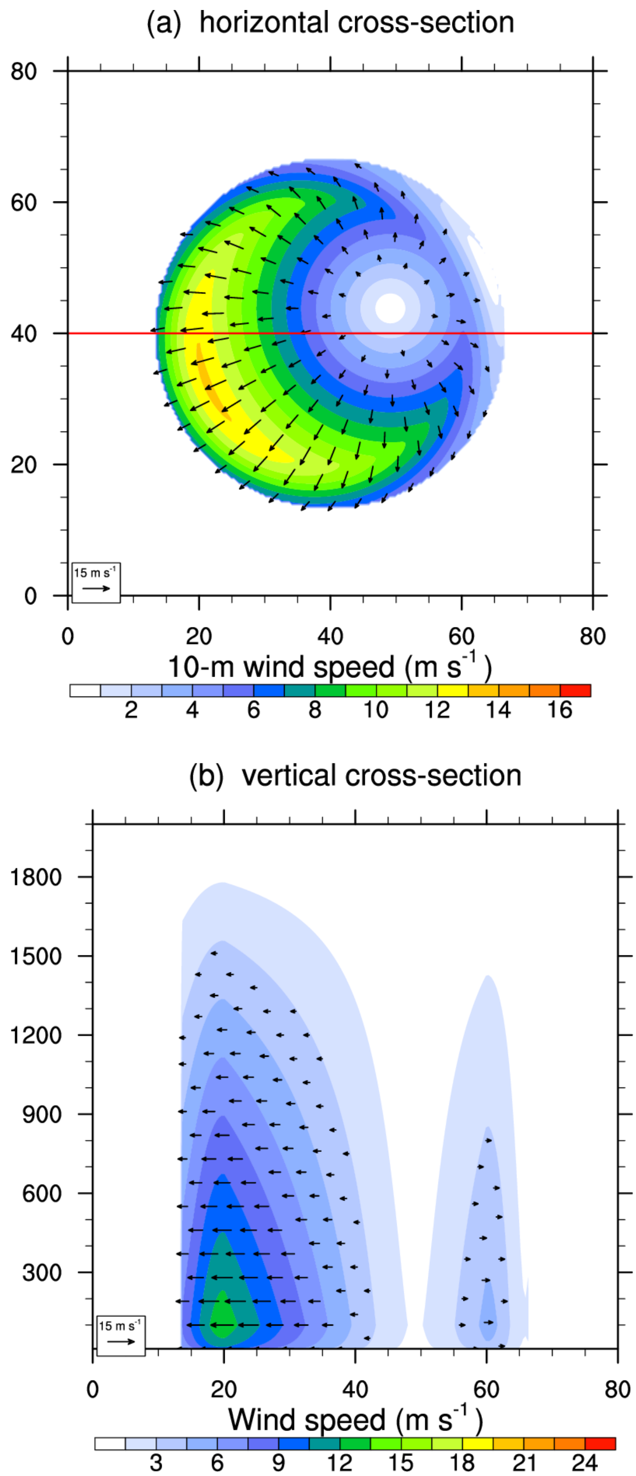

FIG. 9. Parameterization applied to the example of Fig. 8: wind speed (shading, in m s^{-1}) and parallel wind (vectors above 3 m s^{-1} according to the scale) in horizontal (a) and vertical cross-sections (b). Horizontal scales are in km and the vertical scale in m. The red line in (a) shows the trace of (b).

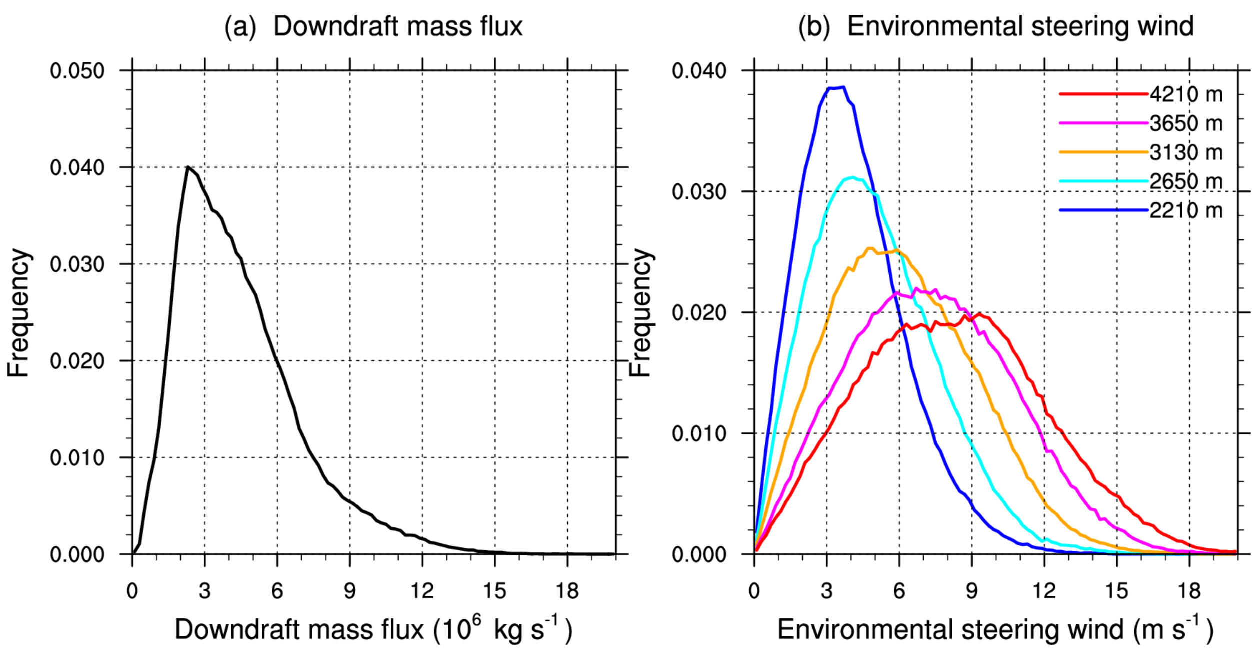

FIG. 10. Probability distribution functions of the downdraft mass-flux M_{dd} (a) and the environmental steering wind U_{env} at different model levels (b) in the 12-km run. Frequencies are computed from 1 June to 30 July 2006 over the area indicated by the boxes in Fig. 11 and where M_{dd} is positive only.

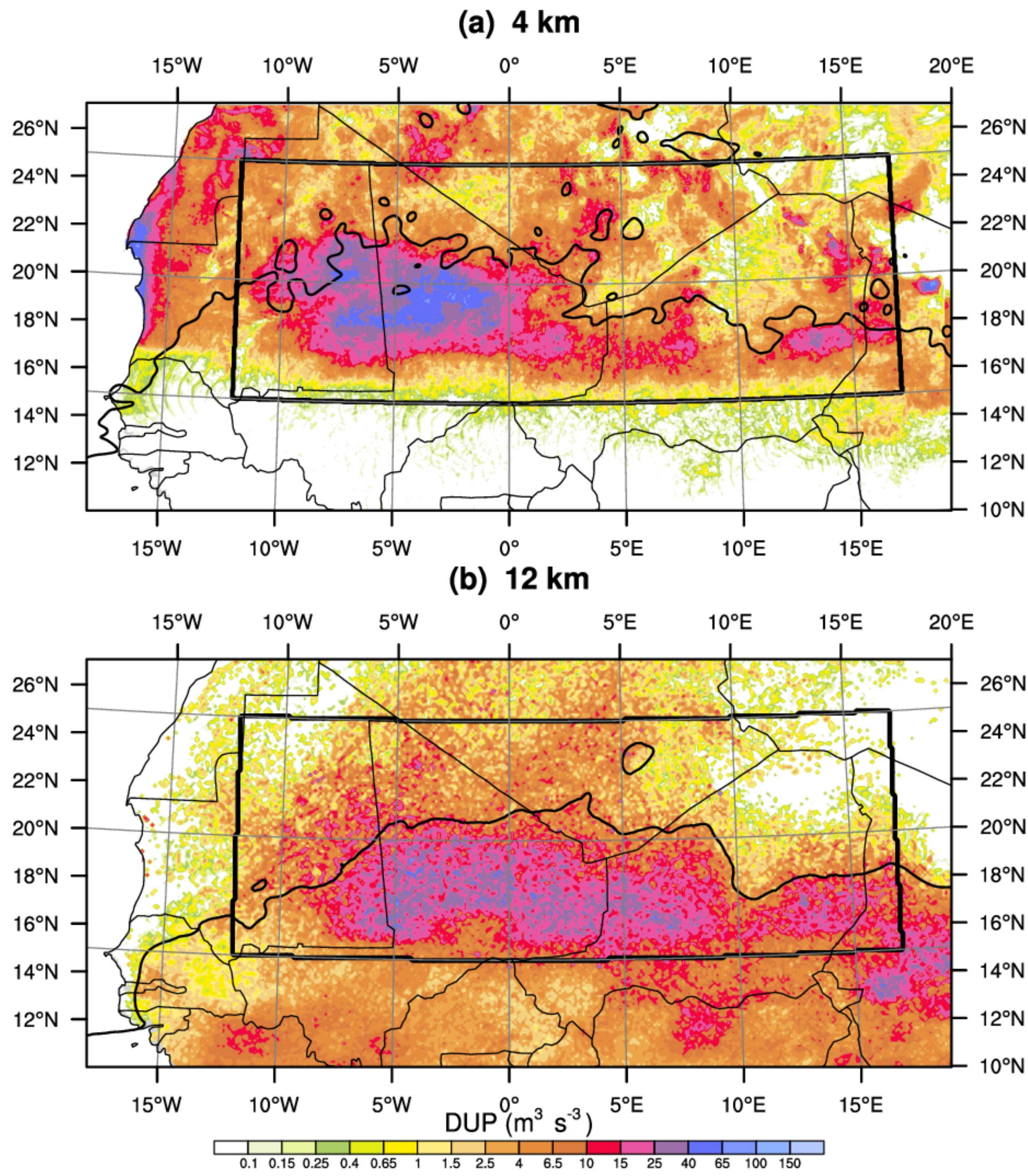

FIG. 11. Dust uplift potential from convective dust storms (shading, in $m^3\ s^{-3}$) and precipitation (smoothed contour at 20 mm) averaged from 1 June to 30 July 2006 in the 4-km (a) and 12-km runs (b). Convective dust storms are identified in the 4-km run (a) and parameterized in the 12-km run (b). The boxes show the area used to compute the diurnal cycle in Fig. 12.

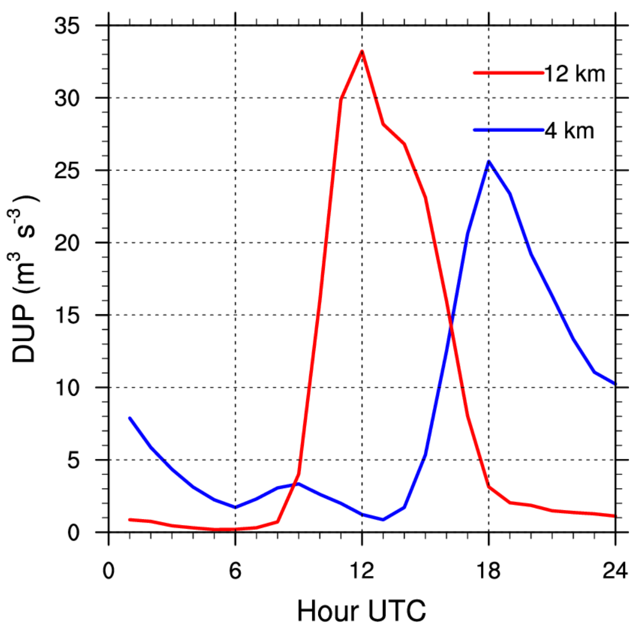

FIG. 12. Diurnal cycle of dust uplift potential from convective dust storms identified in the 4-km run (blue curve) and parameterized in the 12-km run (red curve). The dust uplift potential is averaged from 1 June to 30 July 2006 over the area indicated by the boxes in Fig. 11.